A New 1649-1884 Catalog of Destructive Earthquakes near Tokyo and Implications for the Long-term Seismic Process

Elliot D. Grunewald

U.S. Geological Survey
Menlo Park, CA 94025

now at

Stanford University Department of Geophysics
Stanford, CA 94305

Revised for
J. Geophys. Res.
May 16, 2006

Abstract

In order assess the long-term character of seismicity near Tokyo, I construct an intensity-based catalog of damaging earthquakes that struck the greater Tokyo area between 1649 and 1884. Models for fifteen historical earthquakes are developed using calibrated intensity attenuation relations that quantitatively convey uncertainties in event location and magnitude, as well as their covariance. The historical catalog is most likely complete for earthquakes $M \geq 6.7$; the largest earthquake in the catalog is the 1703 M~8.2 Genroku event. Seismicity rates from 80 years of instrumental records, which include the 1923 M=7.9 Kanto shock, as well as inter-event times estimated from the past ~7000 years of paleoseismic data, are combined with the historical catalog to define a frequency-magnitude distribution for $4.5 \leq M \leq 8.2$, which is well described by a truncated Gutenberg-Richter relation with a b-value of 0.96 and a maximum magnitude of 8.4. Large uncertainties associated with the intensity-based catalog are propagated by a Monte Carlo simulation to estimations of the scalar moment rate. The resulting best estimate of moment rate during 1649-2003 is 1.35×10^{26} dyne cm yr^{-1} with considerable uncertainty at the 1σ level: $(-0.11, +0.20) \times 10^{26}$ dyne cm yr^{-1}. Comparison with geodetic models of the interseismic deformation indicates that the geodetic moment accumulation and likely catalog moment release rates are roughly balanced. This balance suggests that the extended catalog is representative of long-term seismic processes near Tokyo, and so can be used to assess earthquake probabilities. The resulting Poisson (or time-averaged) 30-yr probability for $M \geq 7.9$ earthquakes is 7-11%.

1. Introduction

Tokyo is precariously situated near the junction of three tectonic plates and has been devastated by large earthquakes throughout its recorded history. In 1923, more than 140,000 people were killed in the Great Kanto earthquake [Imamura, 1924; Nyst et al., 2005]. In the ensuing years, the population of Tokyo has increased six-fold, making a deeper understanding of the threat of destructive earthquakes especially urgent.

One of the most powerful tools used in earthquake hazard analysis is the record of past earthquakes, which can be used to assess the potential size, rate, and distribution of future earthquakes. Instrumental records of seismicity in Japan are available for only the last century, a temporal snapshot far shorter than the inter-event time of many large earthquakes. On the other hand, historical records of damage caused by earthquakes are remarkably well documented in Japan and extend back several centuries. These eyewitness damage descriptions have been interpreted as numerical intensity data to estimate locations and magnitudes of historical earthquakes in order to extend the Japanese earthquake record [Utsu, 1979; Utsu, 1982; Usami 1994; Usami, 2003; Bakun, 2005].

Intensity data provide useful constraints on the location and magnitude of historical earthquakes, but most previous studies do not adequately convey the significant uncertainties that are also associated with intensity modeling. In this study, I reanalyze historical earthquakes near Tokyo using a relatively new intensity modeling method developed by Bakun and Wentworth [1997] and Bakun [2005], which quantitatively conveys the uncertainties of the intensity data and methods. The resulting catalog can

then be used in conjunction with Japan's instrumental catalog and rich paleoseismic record to understand the long-term character of seismicity near Tokyo.

2. Intensity Modeling Methods

Most previous intensity modeling studies have used the isoseismal method to estimate earthquake location and magnitude. In these studies, isoseismal contours are drawn in the region affected by an earthquake to designate areas that observed similar intensities. Earthquake magnitude is then determined as a function of the area A_x, in which observed intensities are above a particular threshold x, and the epicenter is located in the center of the highest intensity observations. Following a massive synthesis of shaking and damage observations, Usami [2003] used the isoseismal method to build an extensive historical catalog of earthquakes in Japan. Despite this landmark accomplishment, the isoseismal method has significant weaknesses. Very often, the quantity and spatial distribution of intensity observations limit the precision with which A_x and the location of the isoseismals can be determined. In addition, the isoseismal method utilizes only a subset of the intensity data and fails to provide a quantitative assessment of uncertainties implied by the entire dataset.

In this study, I use a different method to reanalyze selected earthquakes near Tokyo using intensity assignments from Usami [1994]. Bakun and Wentworth [1997] estimated location and moment magnitude of historical earthquakes in California using empirically derived intensity attenuation relationships. Bakun [2005] extended these methods to Japan and derived regional attenuation models based on the Japan Meteorological Agency (JMA) intensity and magnitude scale using local calibration events. Bakun [2005] developed two different attenuation models; one for shallow,

crustal earthquakes ("Honshu model") and one for lower-attenuation subduction earthquakes, including interplate and intraslab earthquakes ("subducting-plate model"):

$$I_{PRED} = -1.89 + 1.42M_{JMA} - 0.00887\Delta_h - 1.66\log\Delta_h \quad \text{"Honshu"} \tag{1}$$

$$I_{PRED} = -8.33 + 2.19M_{JMA} - 0.00550\Delta_h - 1.14\log\Delta_h \quad \text{"subducting-plate"} \tag{2}$$

where I_{PRED} is the predicted JMA intensity, M_{JMA} is the JMA magnitude, and Δ_h is the slant-distance between the observation site and the hypocenter at depth.

In order to estimate earthquake location and magnitude suggested by an entire set of intensity observations, I apply the same grid search algorithm used by Bakun and Wentworth [1997]. For a grid of trial epicenters I first calculate the trial intensity magnitude, M_i, for each intensity data pair, $M_i = f(I_{JMA,i}, \Delta_{h,i})$ where f is either the Honshu or subducting-plate equation; $I_{JMA,i}$ and $\Delta_{h,i}$ are the intensity observation and slant-distance to the hypocenter at site i, respectively. Then, I calculate the mean of the trial intensity magnitudes, $M_{jma} = mean(M_i)$, and the root-mean-square statistical fit, rms[M_{jma}], for each trial epicenter,

$$rms[M_{jma}] = [rms(M_{jma} - M_i) - rms_0(M_{jma} - M_i)], \tag{3}$$

where

$$rms(M_{jma} - M_i) = \sqrt{\frac{\sum_i [W_i (M_{jma} - M_i)]^2}{\sum_i W_i^2}} \tag{4}$$

and rms_0 (M_{jma}-M_i) is the minimum *rms* (M_{jma}-M_i) in the search grid. W_i is a distance weighting function from Bakun [2005] that forces higher rms values for trial epicenters near conflicting intensity assignments. For locations where rms is low, the trial epicenter achieves relatively consistent M_i from the intensity observations.

Contoured rms[M_{jma}] are related to confidence that the epicenter was located within a contour using Table 5b from Bakun and Wentworth [1999]. The location described by the lowest rms value is termed the intensity center. For all possible locations, the most likely M_{JMA}, hereafter M, is described by the local M_{jma}, with a 1σ uncertainty of ±0.25 [Bakun, 2005].

3. Data

The intensity data used in this study are derived from maps compiled by Usami [1994] in which JMA intensity observations were assigned to towns affected in historical earthquakes. Town names have been converted to global coordinates using modern maps. Ambiguous intensity assignments have also been converted to numerical values according to Table 1. Fifteen earthquakes that occurred between 1649 and 1884 and which have at least two damage-based intensity observations are modeled. Most data before 1649 are too sparse to be modeled with precision. Isoseismal contour maps for earthquakes since 1884 have been compiled by Utsu [1982], but discrete intensity observations have not been published and are not yet available.

The Usami [1994] observations include both intensity data based on physical damage records and felt reports (personal accounts of shaking which can be approximately assigned to likely intensities). Felt data are much less reliable than damage-based intensity observations because they are influenced by extraneous factors, such as the sensitivity of the observers and the time of day when the earthquake occurred. In cases where felt data do not strongly conflict with intensity data, however, felt data can provide tighter constraints on earthquake location. For such earthquakes, felt data are

used to define location confidence contours, but only damage observations are used to calculate magnitude.

A key element in the analysis is the selection of the attenuation relation for each earthquake, which requires judgment. The Honshu model assumes a depth of 5 km, and the subduction model uses a depth of 30 km, an approximate depth of the Philippine Sea Plate in the Kanto region [Ishida, 1992]. All earthquakes with a record of a tsunami are modeled with (2). Earthquakes with no tsunami are modeled as subduction events, (2), if peak intensities are located near the coast; otherwise, (1) is used. For datasets in which intensity data are confined to a small area, I assume that these are relatively small crustal events and use (1) in order to minimize magnitude exaggeration caused by depth assumptions.

4. Results

4.1. The Intensity-based Catalog

Intensity centers for all 15 events analyzed here are shown in Figure 1a. Source parameters are listed in Table 2 with 1σ magnitude uncertainty, and the location and magnitude models are shown in the Appendix. For most earthquakes, the best-fit source parameters determined in this study are in relative agreement with those inferred by the Usami [2003] isoseismal study. In some cases, however, I infer a significantly different location or magnitude. Further, two earthquake in the catalog have insufficient intensity data to be adequately constrained by these methods. Examples of each of these cases are presented below with a brief discussion and in Figure 2:

11 March 1853

Most reports of damage for the 11 March 1853 earthquake come from near the Izu Peninsula (Figure 2a). Usami [2003] concluded M = 6.7 ±0.1 for this earthquake and placed the epicenter at the neck of the Izu Peninsula. Because the highest intensities are near the southern coast, this earthquake is analyzed using (2). The model, shown in Figure 2a, has well bounded location contours with an intensity center close to the Usami epicenter. The best estimate of magnitude, 7.0 (6.8-7.3), is also in agreement with the magnitude proposed by Usami.

31 December 1703 Genroku Earthquake

The 1703 Genroku earthquake was one of the most destructive shocks in Japan's recorded history. Much of the southern Kanto region experienced severe shaking, and a tsunami hit the Izu peninsula, Sagami Bay, and the east coast of the Boso Peninsula. The earthquake also caused uplift of bedrock as high as 6 m along the coast [Shishikura, 2003]. Numerous seismologists have created models for this earthquake using a combination of intensity data, tsunami runup height, and surface fault displacement [Matsuda et al., 1978; Usami, 2003; Shishikura et al., in prep.]. The most comprehensive study by Shishikura et al. [in prep.] models the earthquake as M_w=8.2 (8.05 - 8.25) with slip on three main faults off the coast of the Boso Peninsula.

Equation (2) is used to analyze the intensity data for this earthquake and the resulting model is shown in Figure 2b. The intensity center is located at the mouth of Sagami Bay and the estimated magnitude is 7.7 ± 0.25, much lower than the magnitude calculated in the aforementioned studies. Despite the considerable magnitude underestimation, the 67% confidence-contour for the intensity model does closely outline

fault locations inferred by Shishikura et al. [in prep.]. Bakun [2005] found his attenuation equations were accurate for even very large shocks, including one M=7.3 test earthquake and the great Kanto (M~7.9) shock. Magnitude estimates from intensity observations, however, only reflect high-frequency shaking, while magnitudes calculated from tsunami run-up heights and long-term deformation should represent the total moment release. Therefore in subsequent calculations of moment, magnitude uncertainty estimates for this event are taken directly from Shishikura et al. [in prep] using a uniform probability distribution (M=8.05-8.25).

22 October 1767

On October 22, a strong earthquake was felt across a wide region between Edo (ancient Tokyo) and Sendai, in Northeast Japan. Five aftershocks were felt the same day and one aftershock was felt the following day. Damage occurred around Edo, and surface faulting was reported in a small town between Edo and Sendai [Usami, 2003]. The Honshu equation is used to model this event because intensities are observed well onshore and there is no record of tsunami.

Only two damage-based intensity observations are available for this earthquake and felt reports are conflicting and unreliable. The intensity center location is not constrained by the data but is presumed to have occurred somewhere between the two observations (Figure 2c). The two available data define magnitude contours that indicate M = 7.0 over a broad region of possible epicenter locations around the data, including the location of the Usami [2003] epicenter.

A similarly poor intensity dataset is found for one other event, the 1756 earthquake near Chosi (see Appendix). As in the previous case, the magnitude can be

estimated (M= 6.9-7.1) if the epicenter is assumed to be near the intensity observations as Usami [2003 concluded]. Both of these earthquakes are exceptionally uncertain as a result of insufficient data, and their true uncertainties are underrepresented in these models.

4.2. Magnitude-Frequency Distribution

In general, small earthquakes occur much more frequently than large ones. This relation is characterized by a famous equation of Gutenberg and Richter [1944]

$$\log n(M) = a - bM \tag{5}$$

where *n(M)* is the number of earthquakes larger than magnitude *M*. Kagan [1991] used a modified equation that includes a parameter, M_{max}, for the maximum magnitude at which earthquakes can occur

$$\log n(M) = a - bM - k10^{1.5M} \tag{6}$$

where $k = 10^{-1.5Mmax}$. This is often referred to as a truncated G-R distribution.
If a catalog is consistent with a Gutenberg-Richter (G-R) relationship for earthquakes above a certain magnitude, the catalog is considered complete for earthquakes larger than that threshold. So, I seek to establish the magnitude of completeness, M_c, of the historical catalog.

I determine the magnitude-frequency distribution for an extended catalog, which includes the 1649-1884 intensity-based catalog, a 1885-1922 catalog from Ustu [1982], Japan's 1923-2003 instrumental catalog [JMA] (Figure 3), and data from a 7000-year paleoseismic record. I assume that the intensity-based catalog is not complete for M<6.7, since only three such events exist in this catalog, and determine the rate of earthquakes 4.5≤M<6.7 exclusively from the instrumental catalog. Instrumental M<6.7 data from

1923 are not used since an anomalously high ratio of large to small aftershocks surround the 1923 Great Kanto Earthquake [Hamada, 2001]. The rate of earthquakes $6.7 \leq M \leq 7.4$ is calculated using all available modern and intensity-based data from (1649-2003). Rates for the largest earthquakes, Taisho-type (M~7.9, e.g. 1923 Great Kanto earthquake) and Genroku-type (M~8.2), are determined from paleoseismic records of 17 marine terraces, which were collected by Masuda et al. [1978] and Shishikura et al. [2003 and written correspondence] and statistically analyzed by Parsons [2005]. The inter-event time for $M_{JMA} \geq 7.9$ earthquakes is taken as 403±66 years [2005]. For $M_{JMA} \geq 8.2$ Genroku-type events, the rate reflects the mean inter-event time for the four widest Boso terraces, ~2200 years [Shishikura et al., 2003].

I consider the magnitude-frequency distribution within two regions, a larger box that broadly surrounds Tokyo, and a smaller box covering only the area in which the intensity-based catalog is concentrated (Figure 3). Intensity centers for the 1767 and 1856 shocks lie just outside the northern border of the small box but are included in both because of their location uncertainties. The magnitude frequency distribution for the larger area (Figure 4a) shows an offset between the trend of the $M<6.7$ instrumental data (gray line) and the combined $M \geq 6.7$ data, implying that the intensity-based catalog may fail to capture some $M_{JMA} \geq 6.7$ shocks within this area. In contrast, data from the smaller area (Figure 4b) are well described by the truncated G-R relation over the full $4.5 \leq M \leq 8.2$ range, suggesting that the catalog is more likely to be complete for $M \geq 6.7$ within this smaller area. A least-squares regression of the Kagan [1991] equation determines a b-value of 0.96 and $M_{max}=8.40$. This b-value is slightly higher than the regional value,

b=0.85, determined from 1.5≤M≤5.6 shocks for the period 1986-1996. [Wyss and Wiemer, 1997].

Extending the parameterized Kagan [1991] equation without truncation (dashed lines in Figure 4) would predict higher rates for the largest shocks. This would be appropriate if the catalog undersamples the largest earthquakes because only those events that uplift marine terraces or leave tsunami deposits are recognized.

4.3. Catalog Moment

I calculate the total scalar moment for the catalog period under the assumption that the intensity-based catalog is complete for large events, which dominate seismic moment. Empirical evidence from Katsumata [1996] shows that the difference between M_{JMA} and M_w is usually not significant for shallow earthquakes, though some recent exceptions have been noted (2000 Tottori Earthquake: M_{JMA}=7.3, M_w=6.6 [Furamura et al., 2003]). Since I model all earthquakes with depths less than 30 km and much more significant sources of uncertainty exist in the intensity-based models, M_{JMA} is simply substituted for M_w in the Hanks and Kanamori [1979] equation, $Mo = 10^{1.5(M_w+10.7)}$ dyne cm.

A basic calculation of the catalog moment could be made using the magnitude at the intensity center for each earthquake, 2.7 x 10^{28} dyne cm. However, such an approach fails to incorporate the evident uncertainties in magnitude for each earthquake shown in Figure 2 and the Appendix. Magnitude estimates from the Bakun and Wentworth method contain independent uncertainty, ±0.25 M_{JMA} at the 67%-confidence level [Bakun, 2005], as well as covariant uncertainty with location, since the location of the epicenter will determine the magnitude needed to fit the intensity data.

To propagate these complex uncertainties, I use a Monte Carlo simulation to generate 100,000 realizations of the summed moment for the historical intensity-based catalog. In each Monte Carlo iteration, a probabilistic weighting algorithm chooses one possible realization of location and magnitude for each catalog earthquake. The algorithm is designed so that, for any earthquake, the likelihood that the earthquake will be placed in a particular location corresponds to the confidence-level for that location as defined by model rms[M_{jma}]. Thus, 95% of the time, an outcome location is picked within the 95% confidence contour; 67% of the time, the earthquake is located within the 67% confidence contour. Ten confidence ranges between 50% and 95%, from Table 5b of Bakun and Wentworth [1999], are used to constrain the location. The outcome magnitude for each event is derived from the corresponding model magnitude for the outcome location, but is also subsequently modified according to independent magnitude uncertainties. The 1σ uncertainty, ±0.25 M_{JMA}, is propagated using a random Gaussian number generator so that the final output magnitude has a Gaussian probability distribution centered on the model magnitude.

By the end of one Monte Carlo iteration, the probabilistic outcome algorithm has created one realization of the entire catalog with discrete magnitudes for every event. After creating 100,000 of these pseudorandom catalogs, the scalar moment sum for each catalog, Mo_n, is calculated. More probable results for the moment sum occur more often in the total set of iterations. Therefore, the statistical distribution of all 100,000 Mo_n defines the best estimate and uncertainties of scalar moment represented in the catalog.

The Monte Carlo results show a slightly skewed distribution (Figure 5 inset). A peak is centered near 3×10^{28} dyne cm, but a thin tail extends to over 5.5×10^{28} dyne cm.

The mean (2.95 x 10^{28}) and standard deviation (0.56 x 10^{28}) are sensitive to extreme values and are not ideally representative. When the histogram is grouped into 80 bins, the peak occurs at 2.85 x 10^{28} dyne cm; this value is the most frequent outcome in the set of iterations, and thus the highest-confidence estimate of catalog scalar moment. Sixty-seven percent of the outcomes centered on this peak range from 2.41 to 3.50 x 10^{28} dyne cm; the 95% confidence range is 2.00 to 4.16 x 10^{28} dyne cm.

The scalar moment sum is next corrected for the missing M≤6.7 shocks. Because the intensity-based catalog is not complete for earthquakes M<6.7, the moment contribution from these events is not included in the above calculation. This missing moment can be approximated, however, by translating the G-R relation from a magnitude-frequency relation to a moment-frequency relation and integrating this new function from -∞ to Mo(M=6.7) following Andrews and Schwerer [2000]. Using the G-R equation for the area of completeness, the moment contribution from events M<6.7 is calculated as 4.76 x 10^{27} dyne cm for the 235-year period (1649-1884), or 16% of the total moment. Therefore, the best estimate of total scalar moment for 1649-1884 is 3.33 (-0.4, + 0.7) x 10^{28} dyne cm (1σ). Incorporating the moment contribution from the 1885-1922 Utsu [1982] catalog and the 1923-2003 instrumental catalog (inner box, Figure 3) yields an average moment rate of 1.35 (-.11, + .20) x 10^{26} dyne cm yr^{-1}(1σ) from 1649-2003 (Figure 5).

The moment rate and uncertainty is dominated by the largest event in the historical catalog, the 1703 Genroku Earthquake (Mo=1.3-2.7 x 10^{28} dyne cm). The Shishikura et al. [in prep.] model for Genroku is used in place of the intensity-based model (Figure 2b) for the Monte Carlo simulation because it incorporates the entire suite

of available data including tsunami run-up heights and surface fault displacement. Genroku contributes 75-95% of the total 1649-1884 moment; the 1923 Great Kanto earthquake (M=7.9) represents another 20%. The second largest event in the intensity-based catalog, the 1855 Ansei-Edo earthquake (M=7.1-7.6), accounts for only ~3% of the long-term moment rate; this and several other large events in the catalog (Figure 6) contribute the remaining uncertainty.

5. Discussion

5.1. Comparison with the Usami [2003] catalog and isoseismal methods

The catalog proposed in this study differs significantly from that of Usami [2003] (Figure 1). Magnitudes for most earthquakes calculated here are greater than the Usami [2003] magnitudes; the mean increase is 0.3 M_{JMA} units. In addition, inferred epicenters from this study are less tightly clustered around Tokyo and suggest a more dispersed region of seismicity, consistent with the instrumental catalog (Figure 3). Perhaps the more important difference, though, is that this catalog describes the uncertainty and covariance between location and magnitude for these important earthquakes. Rather than suggesting a single location and magnitude estimate for each event, the resulting plots imply a probability distribution of magnitude and location which can be more useful in risk analyses. The uncertainties conveyed here have meaning both for individual earthquakes and the collective catalog. Figure 6 shows combined confidence contours and magnitude uncertainty ranges for the largest, most important events in the catalog.

It is not possible to conclude that the precise source parameters determined in this study are more accurate than those found by Usami [2003]. However, the intensity-attenuation relations are calibrated to modern Japanese earthquakes and have been shown

to be highly accurate [Bakun, 2005]. Further, the Bakun and Wentworth [1997] method has several statistical advantages. Unlike isoseismal constructions, the Bakun-Wentworth method uses the full set of intensity observations and the misfit or inconsistency of the observations with the attenuation model is explicitly used to determine confidence in location and magnitude. This method provides meaningful estimates of source parameters even when data are very sparse and cannot be used to outline isoseismal areas. Further, calculations by this method are reproducible; they are less dependent on subjective judgments common to isoseismal analyses in which contours must be extrapolated offshore or into regions of missing or inconsistent data.

The Bakun-Wentworth method can be applied objectively, in part, because of simplifications in the intensity-attenuation models which represent predicted intensity observations as a function of only two parameters: magnitude and distance from a point-source. The point-source simplification is likely to result in some location error but not magnitude error. The location of the intensity center corresponds to the moment centroid [Bakun, 2005], which is not necessarily the location of the epicenter and may differ by several tens of kilometers for an M~7 earthquake. Magnitude error caused by the point-source approximation is plausible for very large earthquakes for which high intensity observations that are far from the intensity center may be close to the rupture plane, and so predict an erroneously high magnitude for the distant point source. However, the two largest events modeled by Bakun [2005], the 1923 great Kanto M=7.9 earthquake and an M=7.3 shock in 1930, do not overestimate magnitude.

The [2005] equations also simplify energy radiation and attenuation as isotropic effects and so neglect the anisotropic nature of the structures on which these earthquakes

occur. For example, a subducting plate that acts as a waveguide will alter the distribution of intensities and cause error in magnitude and location estimates. In a regional sense, uncertainty introduced by these effects should be represented on average by the location confidence contours and magnitude uncertainty developed by Bakun [2005]. However, corrections can be applied locally, as discussed in the following section, in cases where a systematic bias is identified.

5.2. Intensity Center vs. Epicenter Bias

The intensity centers locations determined in this study are the best approximation based on the historical intensity data and the calibrated Bakun [2005] attenuation models. However, modern Kanto earthquakes indicate that the highest intensities are typically registered ~25 km northwest of the epicenter for earthquakes around Tokyo Bay and the Boso Peninsula (Figure 7) [JMA]. One physical explanation for this bias is that waves traveling north down the Philippine Sea plate slab or west down the Pacific plate slab propagate with lower attenuation and thus shift the locus of strongest shaking [Nakamura et al., 1994]. Secondly, shallow alluvial deposits extending along the western margin of Tokyo Bay and northwest of Tokyo amplify shaking, and so all sources produce higher intensity observations at these sites (see Figure 7 in Stein et al., 2006). Further, for historical intensity datasets, there is a sampling bias because of the concentration of observations at population centers near Tokyo and Yokohama.

To quantify the intensity center-epicenter shift, I use 20 recent earthquakes from the Kanto area, for which dense intensity observations and precisely located epicenters are available. Measuring the distance from the epicenter to the center of the highest intensities for each earthquake, I find that intensity observations are biased to the west by

20.5 ± 11.5 km and to the north by 16.0 km ± 8.9 (1σ) (Table 3). Since it is likely that this bias influences the location of intensity data for the historical earthquakes, inferred epicenters for the historical catalog are located 20.5 km to the east and 16.0 km south of the original intensity centers (Figure 1b). Magnitude estimates are also likely to be influenced by local amplification, especially when intensity data are very sparse (e.g. 1767), but because this effect cannot be quantified for each datum location, no magnitude correction is applied. This analysis therefore does not change the moment calculation or the magnitude-frequency distribution. Similar location biases may exist in other regions of Japan, but no offset is applied to the four earthquakes near the Izu Peninsula because recent earthquakes in this region do not exhibit a significant systematic bias.

5.3. Possible Slow Slip in the 1703 Genroku Shock

The Bakun [2005] attenuation relations determine a much lower magnitude for the 1703 Genroku shock than the Shishikura et al. [in prep.] model, which incorporates ancillary data from tsunami run-up heights and coastal deformation. Because intensity observations only reflect high-frequency shaking, this underestimation of magnitude suggests that the Genroku shock may have been accompanied by a large component of slow slip, as was seen in the 1992 Nicaragua tsunami earthquake (M_w=7.6; M_s=7.0) [Kanamori and Kikuchi, 1993]. Slow earthquakes have been recorded east of the Boso Peninsula [Ozawa et al., 2003] and Linde and Sacks [2002] found that the 1944 Tonakai and 1946 Nankaido earthquakes along the Nankai trough were probably preceded by slow slip events. If slow slip was significant in the 1703 Genroku event, coastal deformation models may overestimate the hazards posed by a similar earthquake.

5.4. The Gutenberg-Richter Relation at Large Magnitudes

The truncated G-R relation determined here (Figure 4b) suggests that the intensity-based catalog is complete for large events. An alternative possibility is that the distribution is not truncated, or at least is not truncated at M=8.4, in which case the catalog would be missing more than half of the expected M~8 shocks (see dashed versus solid black lines in Figure 4). If some of the largest shocks were located far offshore, they may have escaped detection. There is, for example, an unlocatable 1677 shock [Usami, 2003] which triggered a tsunami and caused 246 drownings on the Boso peninsula, and so could be an M~8 event far offshore [Earthquake Research Committee, 1998]. Additionally, there may be great offshore earthquakes in this area with inter-event times longer than the historical record and for which a paleoseismic proxy such as marine terraces has not been identified. However, the smaller box in particular does not extend far offshore, and so should not suffer from this problem. Also, the M_{max} parameter is not simply defined by the largest event in the catalog (M=8.2) but by gradual tapering throughout the higher magnitude range. Thus, it seems more likely that the distribution, in fact, is truncated.

The parameterized Kagan [1991] equation describes the magnitude-frequency distribution with continuity for $4.5 \leq M \leq 8.2$. Although the largest earthquakes in the catalog are characteristic in the sense that earthquakes of similar size recur on one fault or fault segment, they conform to the G-R distribution, rather than what is sometimes termed a characteristic earthquake distribution [Schwartz and Coppersmith, 1984], which would predict higher rates of the largest events. The Kanto catalog distribution stands in contrast to results from Wesnousky [1994], who found that most faults in California

exhibit a characteristic earthquake distribution when inter-event times for the largest events are considered. However, many inter-event times from Wesnousky [1994] are based on more limited historical and paleoseismic data, whereas the data used for this study from Shishikura et al. [in prep.] and Parsons [2005] are based on a ~7000 year record of 17 great earthquakes.

5.5. Moment balance with current strain rates

The 1649-2003 extended catalog can be used to compare the long-term rate of seismic moment release with current moment accumulation rates inferred from geodetically-measured strain rates. Between earthquakes, elastic strain accumulates on faults as the two plates lock together and flex to accommodate plate motion. This accumulating elastic strain is recovered in earthquakes when the fault ruptures and the plates slide quickly past one another. Over a sufficiently long period of time, interseismic elastic strain should be balanced by seismic slip if we ignore any minor component of permanent strain, manifest in uplifted terraces along the Boso coast.

Interseismic elastic strain in a subduction zone can be modeled as back-slip in the opposite direction of plate motion; this back-slip can be regarded as a slip deficit that is recovered during earthquakes [Savage, 1983]. Nishimura and Sagiya [submitted 2006] inverted GPS and leveling data to calculate interseismic slip deficit rates in the Kanto area (Figure 8). In order to compare these results with catalog moment release, the slip deficit rates are related to the rate of seismic moment accumulation according to the dislocation theory of faulting [Burridge and Knopoff, 1964], $\langle u \rangle = Mo / \mu A$, where $\langle u \rangle$ is the average slip over the fault surface, μ is crustal rigidity (taken as 3.8×10^{11} dyne cm^{-2} for regional subduction events [Sato et al., 1998]), and A is the area of fault slip. Table 4

shows conversions of Nishimura and Sagiya [submitted 2006] slip deficit rates to moment accumulation rates. Surface geodesy captures strain from all sources – subduction and crustal. However, the deeper a fault, the more limited the ability to estimate its slip rate, and so surface strain data are biased toward shallow fault sources. Additional uncertainties associated with the moment accumulation rate, mostly due to limited offshore stations, are also listed in Table 4.

Using the portion of Nishimura and Sagiya [submitted 2006] sources within the area of catalog completeness (Figure 8), the moment accumulation rate is 1.33±0.10 x 10^{26} dyne cm yr^{-1}. This rate is in substantial agreement with the with long-term seismic moment rate (Figure 5), 1.35 x 10^{26} dyne cm yr^{-1}, which includes both crustal and subduction sources, implying that regional moment accumulation and moment release are likely balanced over the time span of the catalog. Taken at face value, this balance suggests that the 354-year catalog is representative of the long-term seismic process in the Kanto area. Alternatively, if we assume the catalog is complete and representative, the balance implies that the current rate of strain accumulation typifies the long-term strain rate.

There is, however, an important caveat to the apparent moment accumulation and release balance. Because catalog moment calculations include the entire moment contribution from the 1703 Genroku shock, an earthquake with an inter-event time six times longer than the period of the catalog (~2200 years, [Shishikura et al., 2003]), one would expect the AD 1649-2003 moment rate to exceed strain rate predictions. If instead, only one-sixth of the Genroku moment is included, moment rates would

underestimate the strain predictions by roughly 50%. This moment deficiency, if real, could be due to one or more M~8.0 offshore earthquakes missing from the catalog.

5.6. Earthquake Hazard Probabilities

The G-R equation for the area of completeness defines a Poisson time-averaged probability for earthquakes, $1–e^{-\lambda t}$, during a time interval t, where λ is the rate of earthquakes magnitude M or greater (Figure 9). During an average 30-year period, there is a 57% probability of at least one M≥7.0 shock occurring within the catalog area. A similar probability of 53% is implied by the instrumental catalog in which there are two M≥7.0 earthquakes excluding the 1923 Kanto earthquakes and its aftershocks. If such a large earthquake occurs offshore near the southern boundary of the catalog area, Tokyo may experience only minor damage, but a M=7 in close proximity to the metropolitan area would likely cause significant damage.

Probabilities for M>7.5 shocks differ depending whether the G-R relation is truncated. The probability for a repeated Taisho-type (M=7.9) event is just 7% according to the truncated G-R equation; without truncation this probability rises to 11%. The time-dependent probability for this event is likely to be even lower due to the rather recent occurrence of the Great Kanto earthquake in 1923 in comparison to its mean ~400-year inter-event time. If the G-R relation continues without truncation, there is a 3% probability of an event M>8.5. Although the catalog suggests that such large shocks do not occur, this small probability is an important consequence if the largest shocks in the catalog are undersampled.

6. Conclusions

This study has produced a new historical catalog using intensity assignments from Usami [1994] and the calibrated Bakun [2005] intensity attenuation models for Japan. The catalog provides meaningful estimates of magnitude and location uncertainties and is likely complete for shocks M≥6.7. When merged with modern data, the intensity-based catalog increases the temporal record of significant earthquakes in Japan from the 80-year instrumental period to over 350 years.

The rich ~7000-year paleoseismic record permits one to define a truncated G-R distribution that is consistent over a very wide magnitude range. The rate of moment release for the 1649-2003 extended catalog contains significant uncertainty (-8%, +15%) but is roughly in balance with moment accumulation rates determined from modern geodetic studies. This likely balance and the natural frequency-magnitude distribution suggest that the 1649-2003 catalog is representative of the long-term seismic process near Tokyo, and is thus representative of the style and spatial distribution of seismic sources.

The frequency-magnitude distribution defined in this study can therefore be used to develop earthquake probabilities for future seismicity in the area. The time-averaged 30-year probability for earthquakes M>7.0 is 57%. The time-averaged probability for shocks on the scale of the great 1923 Kanto earthquake is 7-11%, though the time-dependent probability must be much lower. It remains possible, but not likely, that still larger shocks can strike this area and have been missed by the catalog.

Acknowledgements

This work was carried out at the U.S. Geological Survey as part of a broader project to assess Tokyo's seismic hazard. Swiss Re has provided funding for our project and we are grateful for their support. I thank Ross Stein and Bill Bakun of the

U.S. Geological Survey for their valuable assistance and suggestions throughout the course of this study. Bill Bakun has generously shared executable programs for his model algorithms. Serkan Bozkurt of the USGS and Shinji Toda of the Geological Survey of Japan have supplied important data. Translations of some Japanese references have been provided by Ayako Kameda.

References

Andrews, D.J., and E. Schwerer (2000). Probability of rupture of multiple fault segments, *Bull. Seism. Soc. Am.,* **90**, 1498-1506.

Bakun, W. H. (2000). Seismicity of California's north coast, *Bull. Seism. Soc. Am.*, **90***,* 797-812.

Bakun, W. H. (2005). Magnitude and location of historical earthquakes in Japan and implications for the 1885 Ansei Edo earthquake, *J. Geophys. Res.,* **110**, No. B2, B02304, doc:10.1029/2004JB003329.

Bakun, W.H., and C.M. Wentworth (1997). Estimating earthquake location and magnitude from seismic intensity data, *Bull. Seism. Soc. Am.*, **87**, 1502-1521.

Bakun, W. H., and C. M. Wentworth (1999). Erratum to Estimating earthquake location and magnitude from seismic intensity data, *Bull. Seism. Soc. Am.*, **89**, 577.

Earthquake Research Committee (1998). Seismic Activity in Japan, *Headquarters Earthq. Res. Promotion, Tokyo*, English Excerpt, 222 p.

Furumura, T., B.L.N. Kennett, and K. Koketsu (2003). Visualization of 3D Wave Propagation from the 2000 Tottori-ken Seibu, Japan, Earthquake: Observation and Numerical Simulation, *Bull. Seism. Soc. Am.*, **93**, 870-881.

Geological Survey of Japan (2003). Geological Map of Japan 1:1000000 CD-ROM 3rd Edition, *Geological Survey of Japan AIST***.**

Gutenberg, B. and C. F. Richter (1944). Frequency of earthquakes in California, *Bull. Seism. Soc. Am.* **34**, 185-188.

Hamada, N., Y. Kazumitsu, M. Nishwaki, and M. Abe (2001). A comprehensive study of aftershocks of the 1923 Kanto earthquake, *Bull. Seism. Soc. Japan,* **54**, 251-265, (*in Japanese*).

Hanks, T.C., and H. Kanamori (1979). A moment magnitude scale. *J. Geophys. Res.,* **84**, 2348-2350.

Imamura, A. (1924). Preliminary note on the great earthquake of S.E. Japan on Sept.1, 1923, *Seism. Notes of Imp. Earthq. Invest. Comm.,* No. 6.

Ishida, M. (1992), Geometry and relative motion of the Philippine Sea plate and the Pacific plate beneath the Kanto-Tokai District, Japan, *J. Geophys. Res.,* **92**, 489-513.

Japan Meteorological Agency (JMA), Annual Seismological Bulletin, CD-ROM, 2004.

Japan Meteorological Agency (2005). <http://www.jma.go.jp>.

Kagan, Y.Y. (1991). Seismic moment distribution, *Geophys. J. Int.,* **106**, 123-134.

Kanamori, H. and M. Kikuchi (1993). The 1992 Nicaragua earthquake: a slow tsunami earthquake associated with subducted sediments, *Nautre*, **361**, 714-716.

Katsumata, A. (1996). Comparison of magnitudes estimated by the Japan Meteorological Agency with moment magnitudes for intermediate and deep earthquakes, *Bull. Seism. Soc. Am.*, **86**, 832-842.

Linde A.T. and Sacks I.S. (2002). Slow earthquakes and great earthquakes along the Nankai trough, *Ear. Planet. Sci. Lett.*, **203**, 265-275.

Matsuda, T., Y. Ota, M. Ando, and N. Yonekura (1978). Fault mechanism and recurrence time of major earthquakes in Southern Kanto district, Japan, as deduced from coastal terrace data, *Geol. Soc. Amer. Bull.*, **89**, 1610-1628.

Nakamura, R., K. Shimazaki, and T. Hashida (1994). 3-D attenuation structure beneath the Japanese Islands by tomographic inversion of seismic intensity data and predicting JMA intensity distribution in a broad area, *J. Seism. Soc. Japan (Zisin)*, **47**, 21-32 (in Japanese).

Nishimura, T., and T. Sagiya (in preparation). Crustal block kinematics around the northern Philippine Sea plate, central Japan, estimated from GPS and leveling data.

Nyst, M., T. Nishimura, F. F. Pollitz, and W. Thatcher (2005), The 1923 Kanto earthquake re-evaluated using a newly augmented geodetic data set, *submitted to J. Geophys. Res*.

Ozawa, S., S. Miyazaki, Y. Hatanaka, T. Imakiire, M. Kaidsu, M., Murakami (2003). Characteristic silent earthquakes in the eastern part of the Boso peninsula, central Japan, *Geophys. Res. Lett.*, **30**, doi: 10.1029/2002GL016665.

Parsons, T. Significance of stress transfer in time-dependent earthquake probability calculations. *J. Geophys. Res.,* **110***,* doi:10.1029/2004JB003190.

Sato, T., R.W. Graves, P.G.Somerville, and S. Kataoka (1998). Estimates of regional and local strong motions during the great 1923 Kanto, Japan, earthquake (Ms 8.2), *Bull. Seism. Soc. Am.* **88**, 206-227.

Savage, J. C. (1983). A dislocation model of strain accumulation and release at a subduction zone, *J. Geophys. Res.,* **88***,* 4984-4996.

Schwartz, D.P. and K. J. Coppersmith (1984). Fault behavior and characteristic earthquakes: examples from the Wasatch and San Andreas fault at Pallett Creek, *J. Geophys. Res.* **97**, 12457-12470.

Shishikura, M. (2003). Cycle of interplate earthquakes along the Sagami Trough deduced from tectonic geomorphology, *Bull. Earthq. Res. Inst. Univ. Tokyo,* **78**, 245-254.

Shishikura, M., S. Toda, and K. Satake (in preparation). Fault model of the 1703 Genroku Kanto earthquake (M=8.2) along the Sagami Trough deduced from renewed coseismic crustal deformation.

Stein, R. S., S. Toda, E. Grunewald (2006). A new probabilistic seismic hazard assessment for greater Tokyo, *Proc R. Soc. A*., (in press).

Usami, T. (1994). Seismic intensity maps and isoseismal maps of historical earthquakes of Japan, *Japan Electric Asssociation*, 1994.

Usami, T. (2003). Materials for Comprehensive List of Destructive Earthquakes in Japan, [416]-2001, *University of Tokyo Press*, 605 pp., (in Japanese).

Utsu, T (1982). Catalog of large earthquakes in the region of Japan from 1885 through 1980, *Bull. Earthq. Res. Inst. Univ. Tokyo,* **57**, 401-463, (in Japanese).

Utsu, T., (1979). Seismicity of Japan from 1885 through 1925 – a new catalog of earthquakes of M≥6 felt in Japan and smaller earthquakes which caused damage in Japan, *Bull. Earthq. Res. Inst. Univ. Tokyo,* **54(2)***,* 253-308, (in Japanese).

Wesnousky, S. (1994). G-R or characteristic earthquake distribution, Which is it?, *Bull. Seism. Soc. Am.*, **84**, 1940-1959.

Wyss, M., and S. Wiemer (1997). Two current seismic quiescences within 40 km of Tokyo, *Geophys. J. Int.,* **128**, 459-473.

Figure 1. Three versions of the 1649-1884 intensity-based catalog. (a) Intensity centers determined in this study using Bakun [2005] intensity attenuation models (highly uncertain events dashed). (b) Epicenters inferred from intensity center-epicenter shift. (c) Usami [2003] epicenters.

Figure 2. Example models for three catalog earthquakes. Dashed contours are M_{jma} and solid contours are the 67% and 95% location confidence contours where shown. The triangle is the location of the intensity. (a) The 1853 event. (b) The 1703 Genroku shock (unrevised; revised M_{jma} contours increased by 0.4). (c) The 1767 event.

Figure 3. Earthquakes from other catalogs used in this study. Dashed circles are $M \geq 6.7$ from the 1885-1922 Utsu [1982] catalog. Solid circles are $M \geq 5.0$ for the 1923-2003 catalog [JMA]. The dashed box is the region of completeness for the intensity-based catalog.

Figure 4. Frequency-magnitude distribution for (a) the broader Kanto area (Fig. 3 outer box) and (b) the area of completeness (Figure 3, inner box). Rates for $M<6.7$ are from the instrumental catalog (1924-2003). Rates for $6.7 \leq M \leq 7.4$, are from the extended catalog (1649-2003). Rates for Taisho-type and Genroku-type events are from paleoseismic data (Parsons, 2005; Shishikura et al., 2003). The solid line is the least-squares truncated G-R Kagan [1991] equation. The dashed line shows the G-R curve without truncation.

Figure 5. Monte Carlo statistics for catalog scalar moment and comparison with moment accumulation rates from geodesy. Inset: Monte Carlo statistics for total scalar moment for the 1649-1884 catalog. Large plot: Light curve shows the relative confidence for the

1649-2003 seismic moment rate. The dark band is the moment accumulation rate estimated from geodesy [Nishimura and Sagiya, submitted 2006] with 1σ uncertainty.

Figure 6. Uncertainties associated with the largest earthquakes in the 1649-1884 catalog. Colored areas on left are 67% location confidence contours using Bakun [2005] intensity-attenuation models (dashed where constrained by judgment). Concentric circles on right are 1σ confidence range in magnitude (dashed where highly uncertain).

Figure 7. Three examples of modern earthquakes showing systematic bias between the location of the highest intensities and the precisely located epicenter [JMA].

Figure 8. Nishimura and Sagiya [submitted 2006] slip deficit model from recent geodetic data. Dotted lines are the upper edge of the faults. More positive values reflect faster moment accumulation. The green box shows the area of completeness for the historical catalog.

Figure 9. Thirty-year time-averaged probability of earthquakes. Poisson probabilities reflect likelihood that at least one earthquake magnitude M or larger will occur during any 30-year period within the area shown in the inset map. The solid line and dashed line are based on the truncated G-R equation and untruncated G-R equation respectively.

APPENDIX. All fifteen earthquake models in the intensity-based catalog. Dashed contours are M_{jma} and solid contours are the 67% and 95% location confidence contours where shown. The triangle is the location of the intensity. The green star is the location of the Usami [2003] epicenter.

Table 1. Conversion table for Usami [1994] intensity records**.**

Usami (1996) assignment	Numerical value used
Real Data	
"4"	4
"4-5"	4.5
">4"	4.5
"5"	5
"5-(6)"	5.5
"5-6"	5.5
">5"	5.5
"6"	6
"6-7"	6.5
"7"	7
Felt Data	
"e"	3
"E"	4
"S"	5

Table 2. Model parameters and results for the historical catalog earthquakes.

			THIS STUDY						USAMI (2003)		
		Attenuation	Intensity Center		Inferred Epicenter						
Date	# Obs	Model	Lon	Lat	Lon	Lat	JMA Magnitude		Lon	Lat	JMA Mag
07/30/1649	6	Honshu-F	139.75	35.92	139.50	35.76	7.0	(6.7-7.5)	139.5	35.8	7
12/31/1703	83	Subduction-F	139.81	35.18	139.66	35.03	8.2	(8.1-8.2)*	139.8	34.7	7.9-8.2
01/19/1706	6	Honshu-F	139.69	35.8	139.54	35.65	5.9	(5.6-6.7)	139.8	35.6	5.75
02/20/1756	6	Subduction	140.82	35.88	140.67	35.73	6.9	(6.0-7.3)‡	140.9	35.7	5.5-6.0
10/22/1767	8	Honshu	139.86	36.12	139.71	35.97	7.0	(6.0-7.2)‡	139.8	35.7	6
08/23/1782	48	Subduction	139.05	35.13	139.05	35.13	7.2	(7.0-7.6)	139.1	35.4	7
01/01/1791	15	Honshu-F	139.62	35.84	139.47	35.69	5.9	(5.6-6.4)	139.6	35.8	6.0-6.5
04/21/1812	23	Subduction-F	139.77	35.54	139.62	35.39	7.1	(6.8-7.4)	139.65	35.45	6.25
03/09/1843	20	Subduction-F	139.11	35.41	139.11	35.41	6.7	(6.3-6.8)	139.1	35.35	6.5
01/26/1853	59	Subduction-F	139.15	35.31	139.15	35.31	7.0	(6.8-7.3)	139.15	35.3	6.6-6.8
11/11/1855	191	Subduction	139.95	35.65	139.80	35.50	7.4	(7.1-7.6)	139.8	35.65	7.0-7.1
04/11/1856	33	Honshu-F	139.41	36.06	139.26	35.91	6.8	(6.4-7.2)	139.5	35.7	6.0-6.5
01/11/1859	6	Honshu-F	139.65	35.97	139.50	35.82	6.1	(6.0-6.7)	139.7	35.9	6.0-6.5
05/12/1870	8	Subduction-F	139.71	35.19	139.33	35.02	6.8	(6.4-6.9)	139.1	35.25	6
10/15/1884	6	Subduction	139.83	35.91	139.68	35.75	6.7	(6.4-6.8)	139.75	35.7	NA

F felt data used to constrain location

‡ highly uncertain

* from Shishikura et al. [in prep.]

Table 3. Statistics of location bias for intensity observations from recent earthquakes.

					Intensity Bias	
Date	Lat	Lon	Depth(km)	JMA Mag	West (km)	North (km)
2/16/2005	36.03	139.90	45	5.4	-15	5
7/10/2004	36.08	139.88	48	4.7	-5	20
5/31/2001	36.18	139.80	56	4.7	0	15
7/15/1999	35.93	140.43	50	5.0	10	15
4/8/2003	36.07	139.92	47	4.6	15	20
5/12/2003	35.88	140.07	50	4.6	15	15
10/15/2003	35.62	140.05	74	5.1	15	-5
2/23/2005	36.10	139.85	50	4.4	15	15
6/3/2000	35.68	140.75	48	6.0	20	0
7/20/2001	36.17	139.82	55	5.0	20	20
5/17/2003	35.73	140.65	47	5.3	20	10
2/4/2004	36.00	140.08	65	4.2	20	25
4/11/2005	35.57	140.18	73	4.4	20	10
4/11/2005	35.73	140.62	52	6.1	20	15
11/8/1998	35.63	140.03	80	4.7	25	15
9/20/2003	35.22	140.30	70	5.8	20	20
2/8/2005	36.13	140.08	67	4.8	25	15
7/23/2005	35.01	139.96	74	6.1	25	5
8/18/2003	35.80	140.12	69	4.8	30	15
4/17/2005	35.15	139.97	69	4.4	30	15
9/13/1999	35.60	140.17	76	5.1	35	20

Table 4. Moment accumulation rates calculated from the Nishimura and Sagiya [in prep.] slip deficit model.

Source I.D.	Length (km)	Width (km)	Inlcuded (%)	Slip Deficit Rate (mm/yr)	Uncertainty (mm/yr)	Moment Rate (dyne cm/yr)	Uncertainty (dyne cm/yr)
G	24	30	100	16	0.4	4.38E+24	1.09E+23
H	40	35	100	12	0.8	6.38E+24	4.26E+23
I	37	30	100	28	0.5	1.18E+25	2.11E+23
J	37	30	100	22	0.9	9.28E+24	3.80E+23
K	43	33	100	4	0.9	2.16E+24	4.85E+23
L	40	30	100	40	0.8	1.82E+25	3.65E+23
M	40	30	100	26	1.0	1.19E+25	4.56E+23
N	51	35	100	3	0.9	2.03E+24	6.10E+23
O	51	35	75	18	0.8	9.16E+24	4.07E+23
P	30	50	100	48	0.7	2.74E+25	3.99E+23
Q	51	30	60	30	1.0	1.05E+25	3.49E+23
R	51	38	30	41	0.8	9.06E+24	1.77E+23
S	51	35	10	10	0.8	6.78E+23	5.43E+22
BB	30	14.9	100	28	0.7	4.76E+24	1.19E+23
CC	30.5	14.9	100	9	1.5	1.55E+24	2.59E+23
DD	28	14.9	75	31	1.6	3.69E+24	1.90E+23

Figure 1

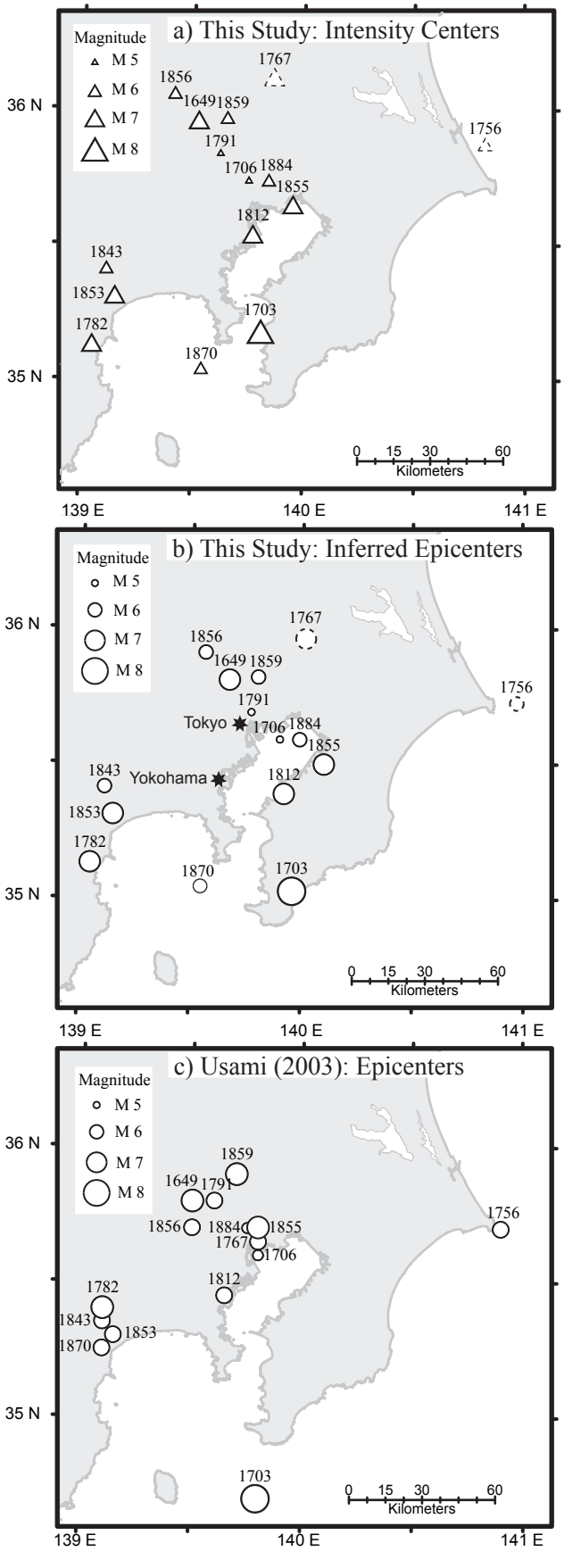
a) This Study: Intensity Centers
Magnitude
M 5
M 6
M 7
M 8
1767
1856
1649
1859
1791
1706
1884
1855
1812
1843
1853
1782
1703
1870
1756
36 N
35 N
0 15 30 60
Kilometers
139 E
140 E
141 E
b) This Study: Inferred Epicenters
Magnitude
M 5
M 6
M 7
M 8
1767
1856
1649
1859
1791
Tokyo
1706
1884
1855
1843
Yokohama
1812
1853
1782
1870
1703
1756
36 N
35 N
0 15 30 60
Kilometers
139 E
140 E
141 E
c) Usami (2003): Epicenters
Magnitude
M 5
M 6
M 7
M 8
1859
1649
1791
1856
1884
1855
1767
1706
1812
1782
1843
1853
1870
1703
1756
36 N
35 N
0 15 30 60
Kilometers
139 E
140 E
141 E

Figure 2

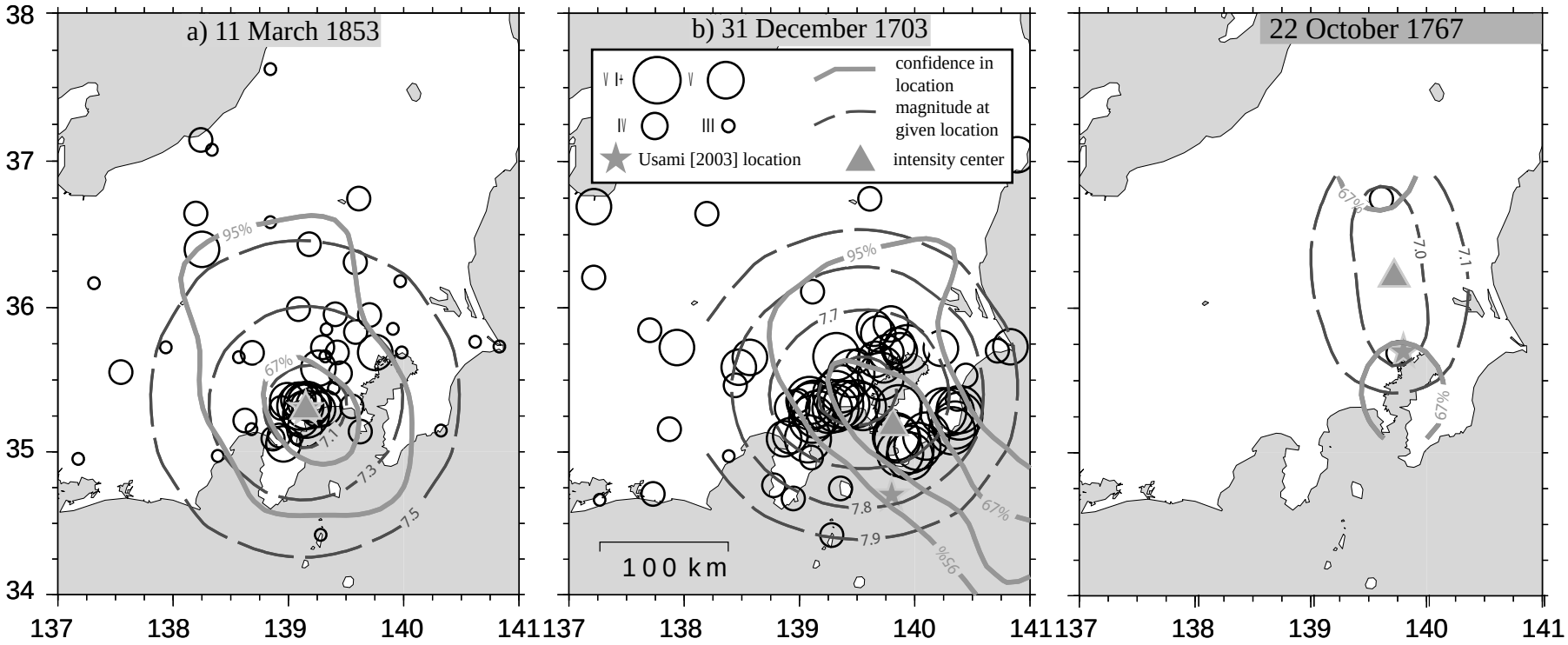
a) 11 March 1853
b) 31 December 1703
22 October 1767
confidence in location
magnitude at given location
Usami [2003] location
intensity center
95%
67%
7.1
7.3
7.5
7.7
7.8
7.9
7.0
100 km
38
37
36
35
34
137
138
139
140
141

Figure 3

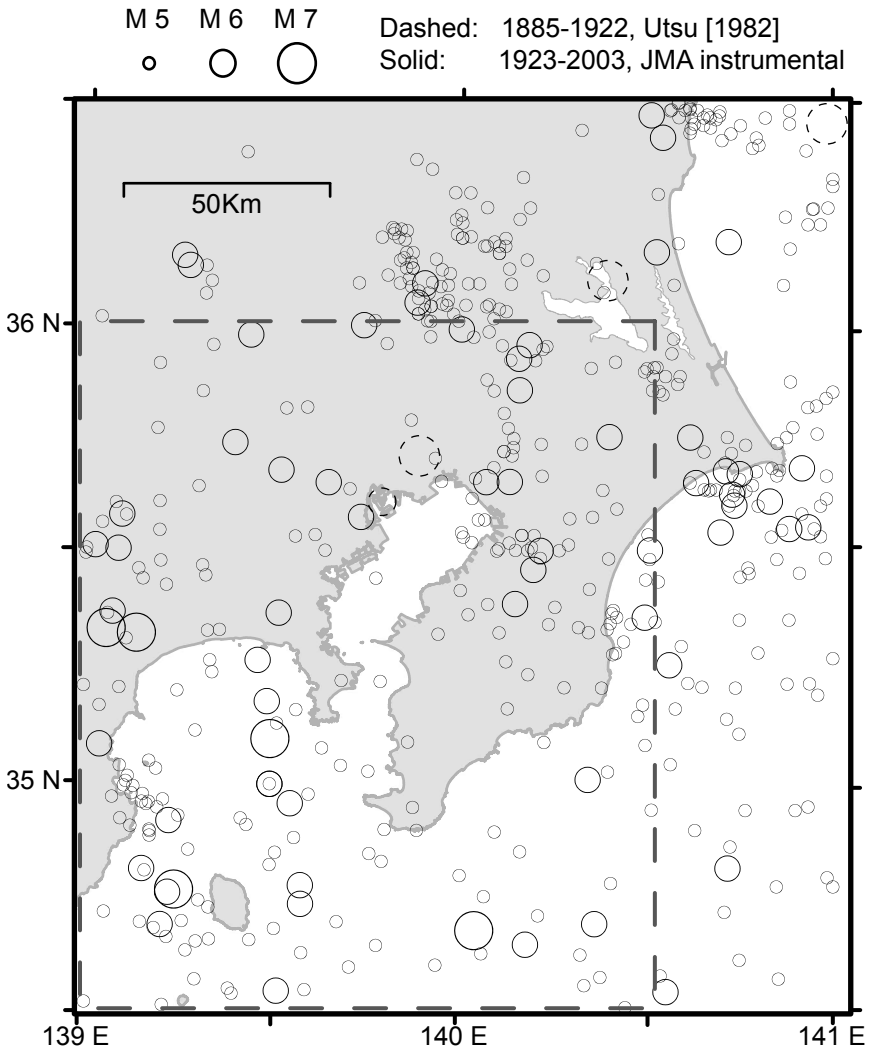
M 5
M 6
M 7
Dashed: 1885-1922, Utsu [1982]
Solid: 1923-2003, JMA instrumental
50Km
36 N
35 N
139 E
140 E
141 E

Figure 4

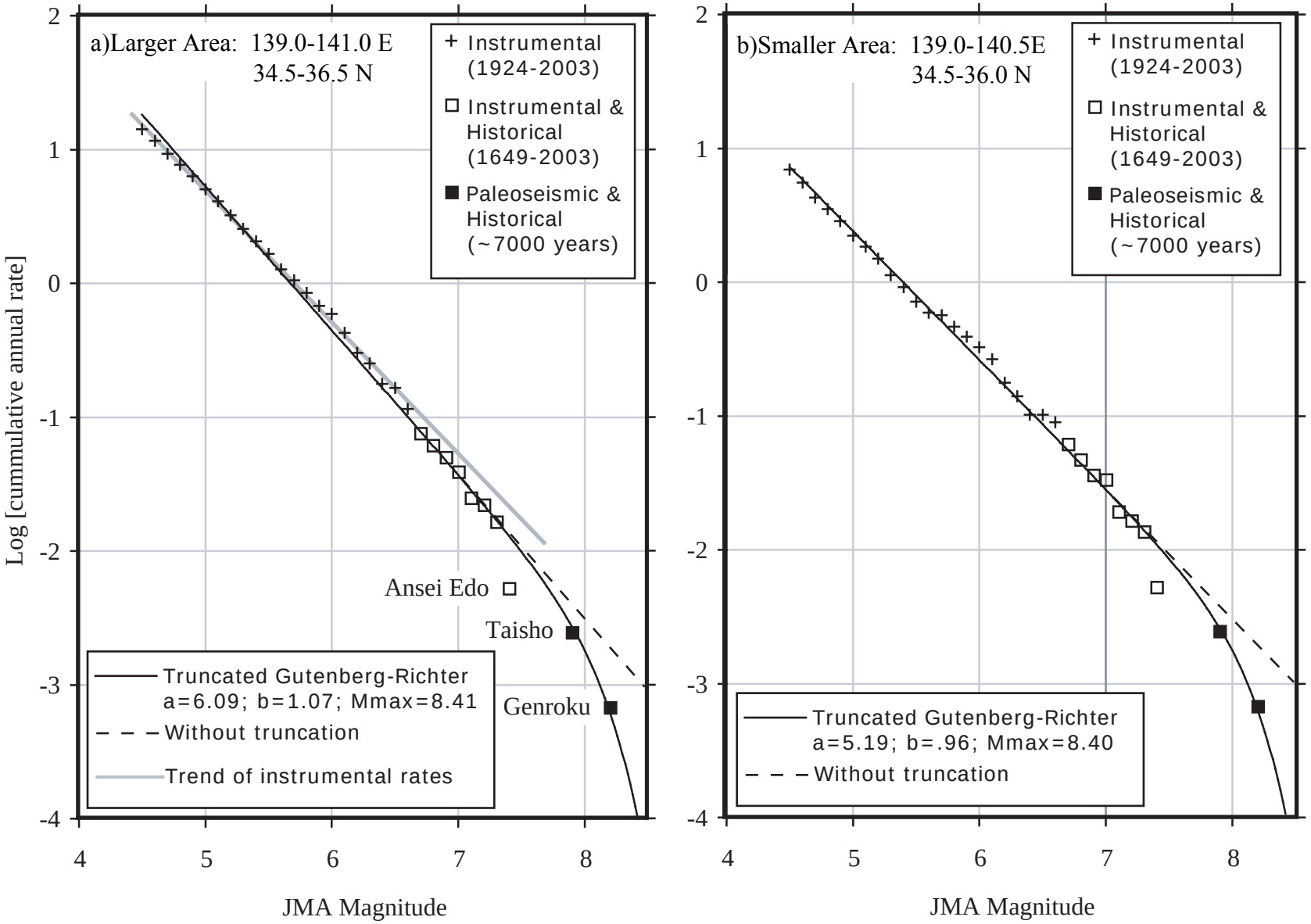
a)Larger Area: 139.0-141.0 E
34.5-36.5 N
+ Instrumental (1924-2003)
□ Instrumental & Historical (1649-2003)
■ Paleoseismic & Historical (~7000 years)
Ansei Edo
Taisho
Genroku
Truncated Gutenberg-Richter
a=6.09; b=1.07; Mmax=8.41
Without truncation
Trend of instrumental rates
Log [cummulative annual rate]
JMA Magnitude
b)Smaller Area: 139.0-140.5E
34.5-36.0 N
+ Instrumental (1924-2003)
□ Instrumental & Historical (1649-2003)
■ Paleoseismic & Historical (~7000 years)
Truncated Gutenberg-Richter
a=5.19; b=.96; Mmax=8.40
Without truncation
JMA Magnitude

Figure 5

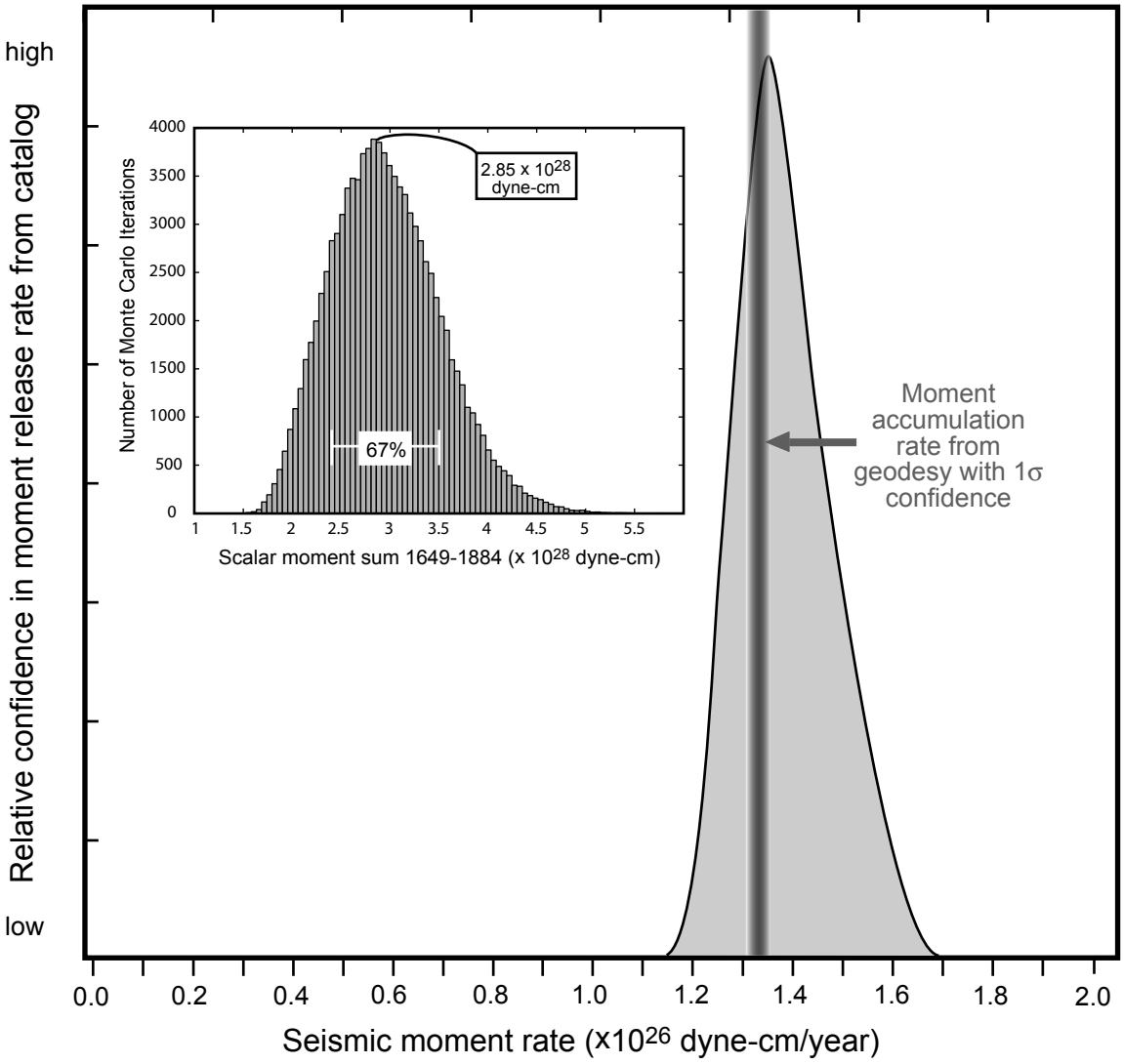
high
low
Relative confidence in moment release rate from catalog
Number of Monte Carlo Iterations
2.85 x 10^28 dyne-cm
67%
Scalar moment sum 1649-1884 (x 10^28 dyne-cm)
Moment accumulation rate from geodesy with 1σ confidence
Seismic moment rate (x10^26 dyne-cm/year)

Figure 6

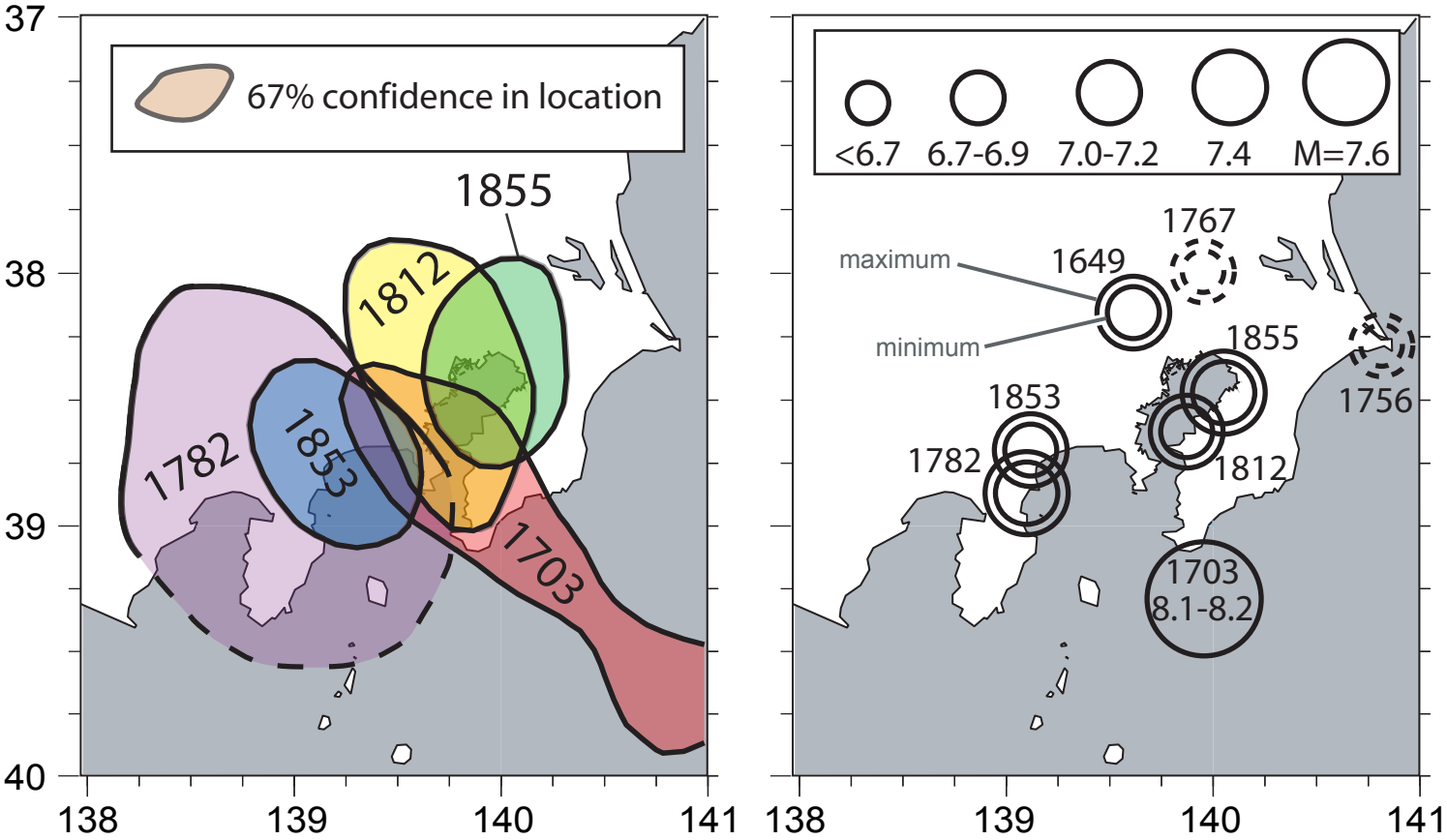
37
38
39
40
138
139
140
141
67% confidence in location
1855
1812
1782
1853
1703
<6.7
6.7-6.9
7.0-7.2
7.4
M=7.6
maximum
minimum
1649
1767
1855
1853
1782
1812
1756
1703
8.1-8.2

Figure 7

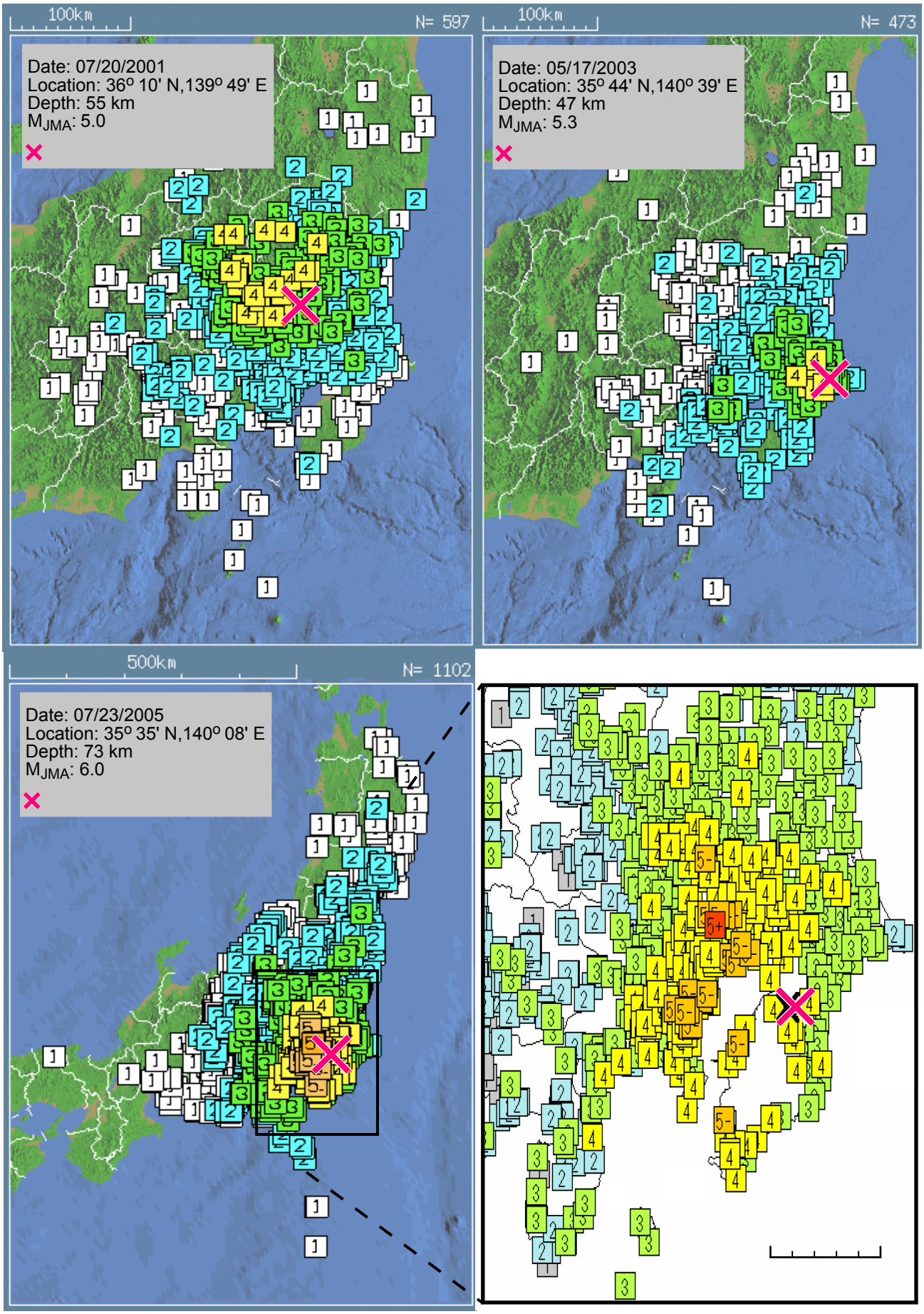
100km
N= 597
Date: 07/20/2001
Location: 36º 10' N,139º 49' E
Depth: 55 km
M_JMA: 5.0
100km
N= 473
Date: 05/17/2003
Location: 35º 44' N,140º 39' E
Depth: 47 km
M_JMA: 5.3
500km
N= 1102
Date: 07/23/2005
Location: 35º 35' N,140º 08' E
Depth: 73 km
M_JMA: 6.0

Figure 8

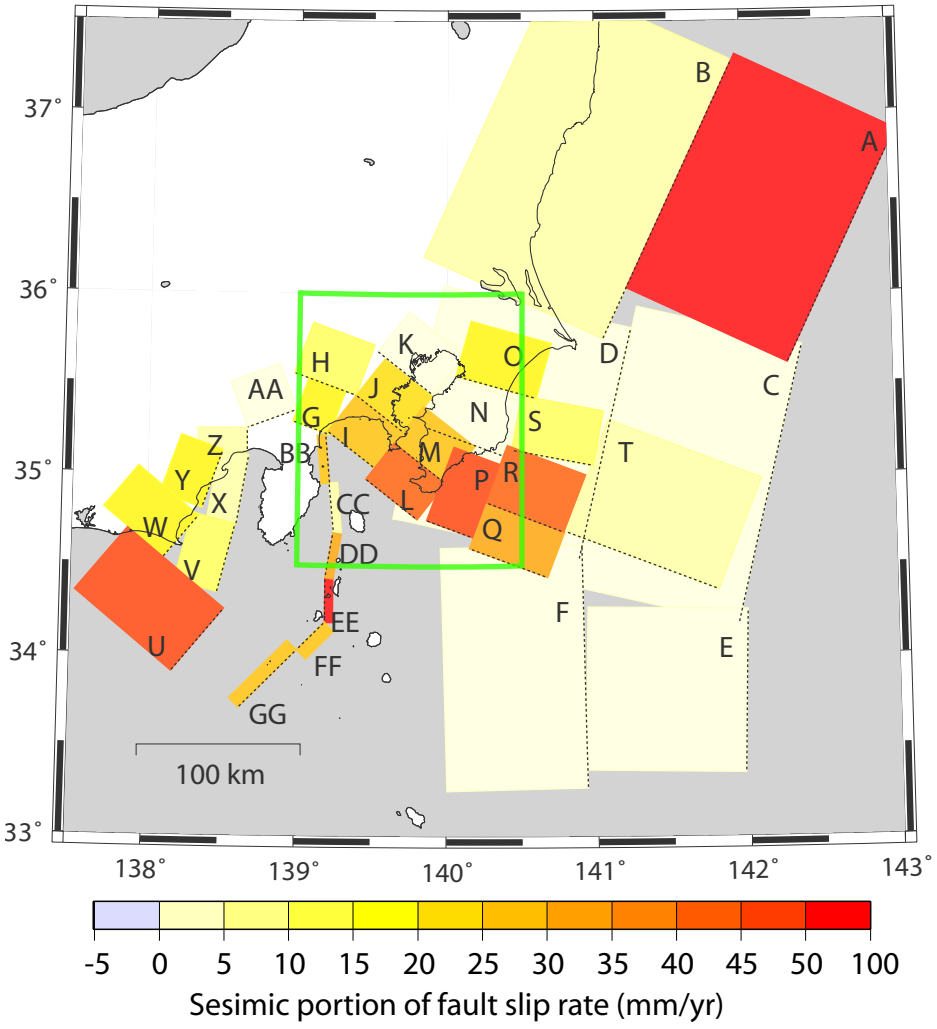
37°
36°
35°
34°
33°
138°
139°
140°
141°
142°
143°
A
B
C
D
E
F
G
H
I
J
K
L
M
N
O
P
Q
R
S
T
U
V
W
X
Y
Z
AA
BB
CC
DD
EE
FF
GG
100 km
-5
0
5
10
15
20
25
30
35
40
45
50
100
Sesimic portion of fault slip rate (mm/yr)

Figure 9

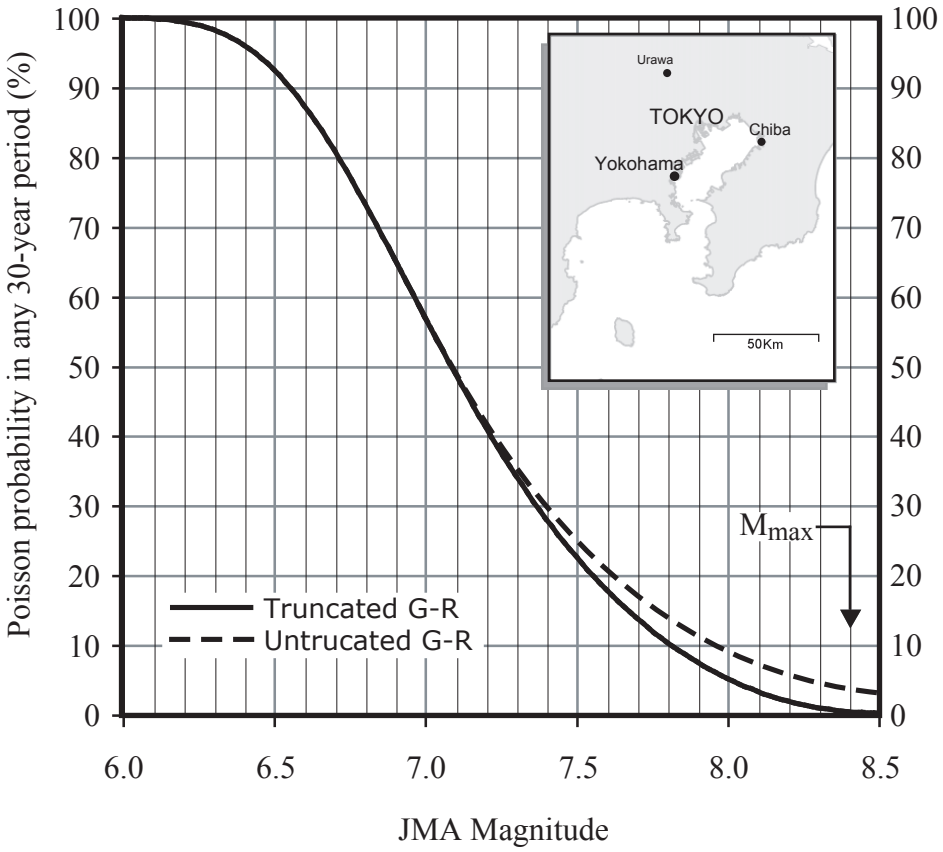
Poisson probability in any 30-year period (%)
100
90
80
70
60
50
40
30
20
10
0
6.0
6.5
7.0
7.5
8.0
8.5
JMA Magnitude
Truncated G-R
Untrucated G-R
M_{max}
Urawa
TOKYO
Chiba
Yokohama
50Km

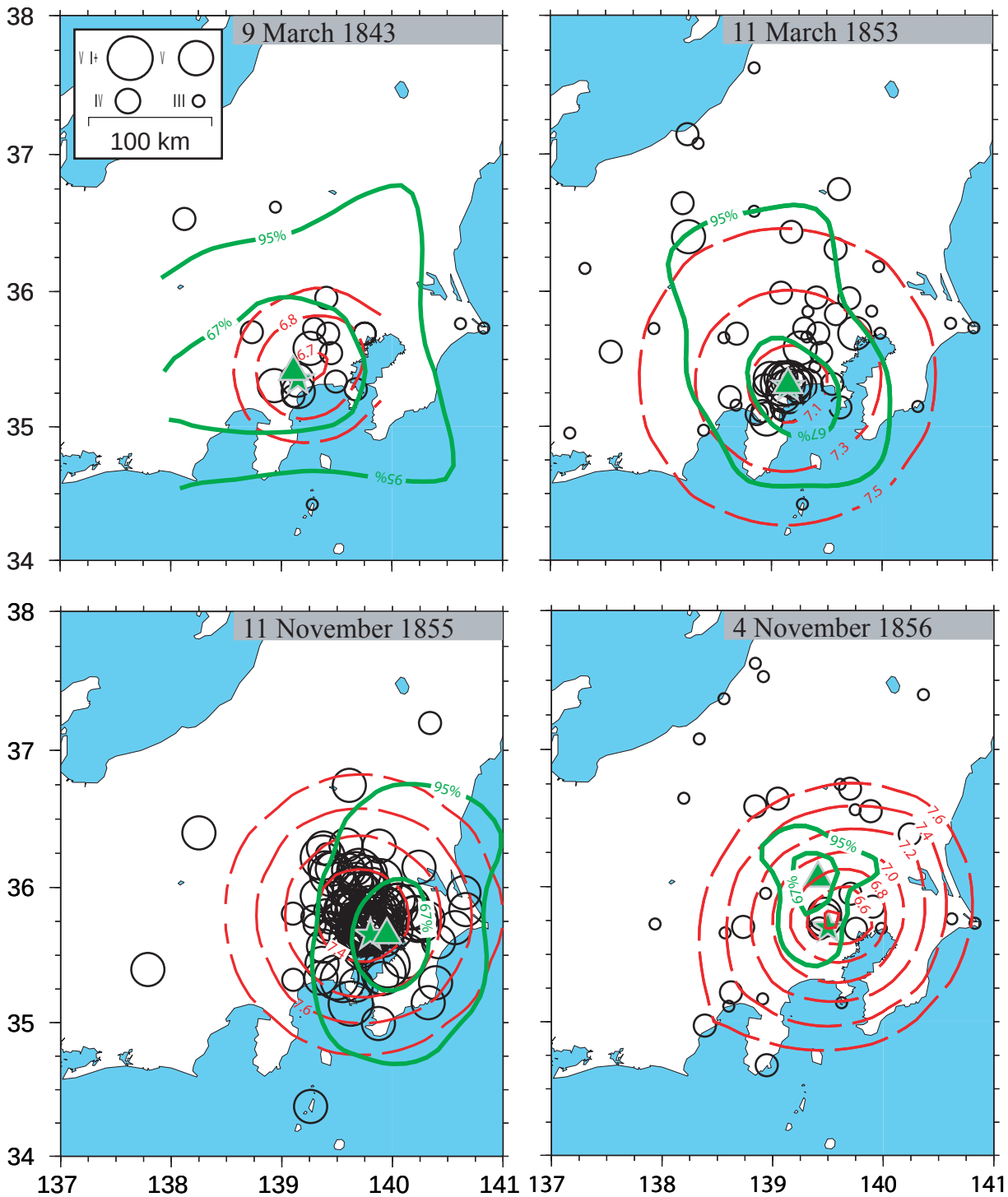
9 March 1843
11 March 1853
11 November 1855
4 November 1856
VI+
V
IV
III
100 km
95%
67%
6.8
6.7
7.1
7.3
7.5
7.6
7.4
7.2
7.0
6.9
38
37
36
35
34
137
138
139
140
141

Figure 1

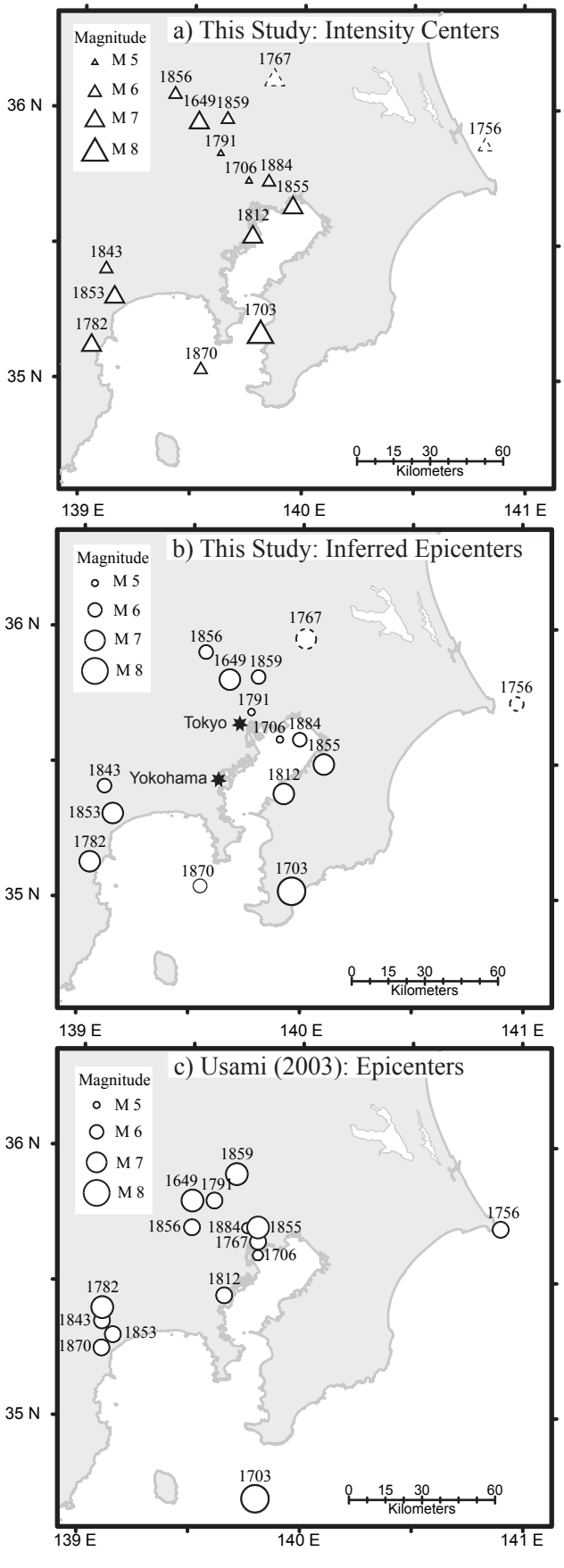
a) This Study: Intensity Centers
Magnitude
M 5
M 6
M 7
M 8
1767
1856
1649
1859
1791
1706
1884
1855
1812
1843
1853
1782
1703
1870
1756
36 N
35 N
0 15 30 60
Kilometers
139 E
140 E
141 E
b) This Study: Inferred Epicenters
Magnitude
M 5
M 6
M 7
M 8
1767
1856
1649
1859
1791
Tokyo
1706
1884
1855
1843
Yokohama
1812
1853
1782
1870
1703
1756
36 N
35 N
0 15 30 60
Kilometers
139 E
140 E
141 E
c) Usami (2003): Epicenters
Magnitude
M 5
M 6
M 7
M 8
1859
1649
1791
1856
1884
1855
1767
1706
1812
1782
1843
1853
1870
1703
1756
36 N
35 N
0 15 30 60
Kilometers
139 E
140 E
141 E

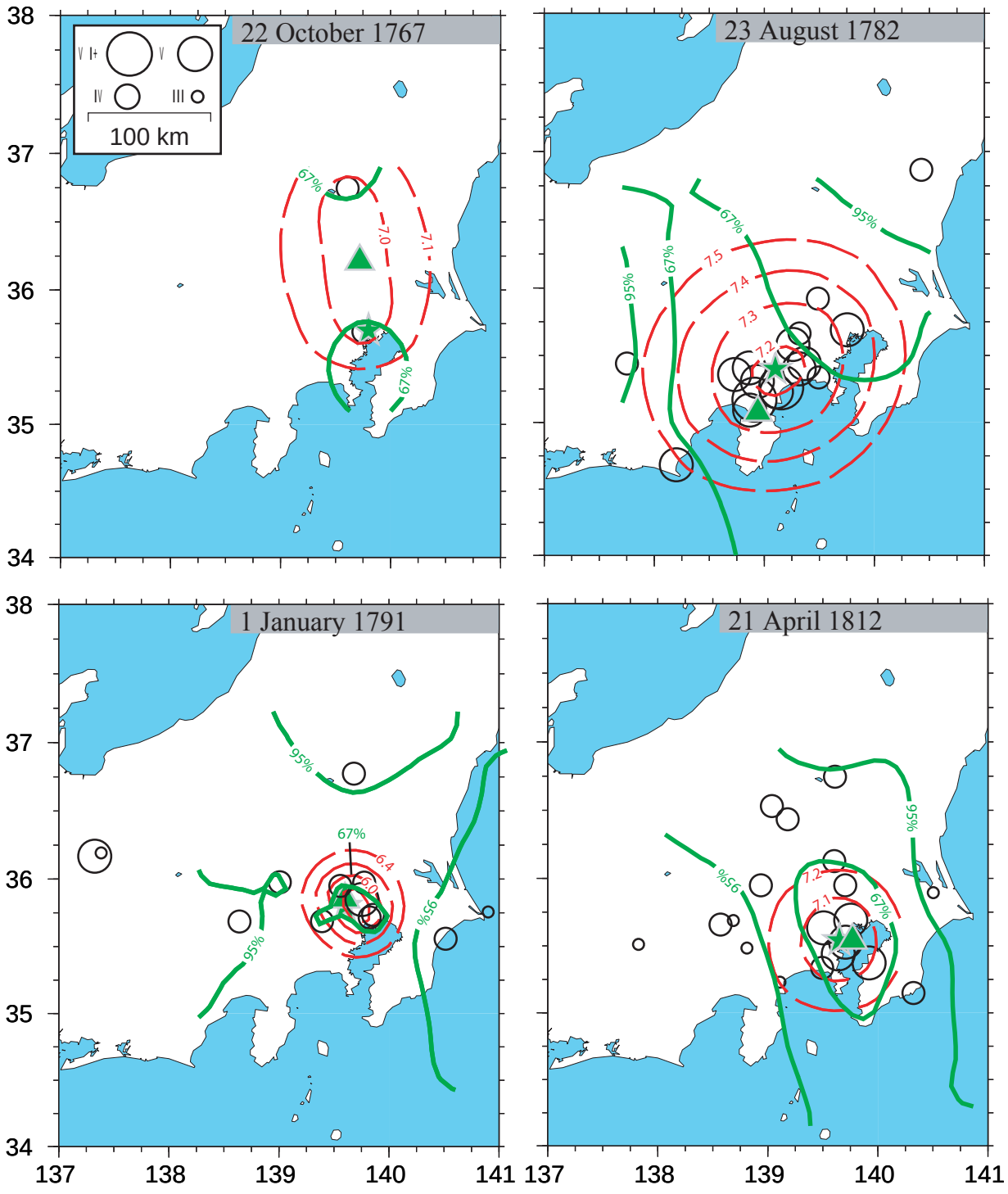
22 October 1767
23 August 1782
1 January 1791
21 April 1812
V I+
V
IV
III
100 km
67%
95%
7.0
7.1
7.5
7.4
7.3
7.2
6.4
6.0
38
37
36
35
34
137
138
139
140
141

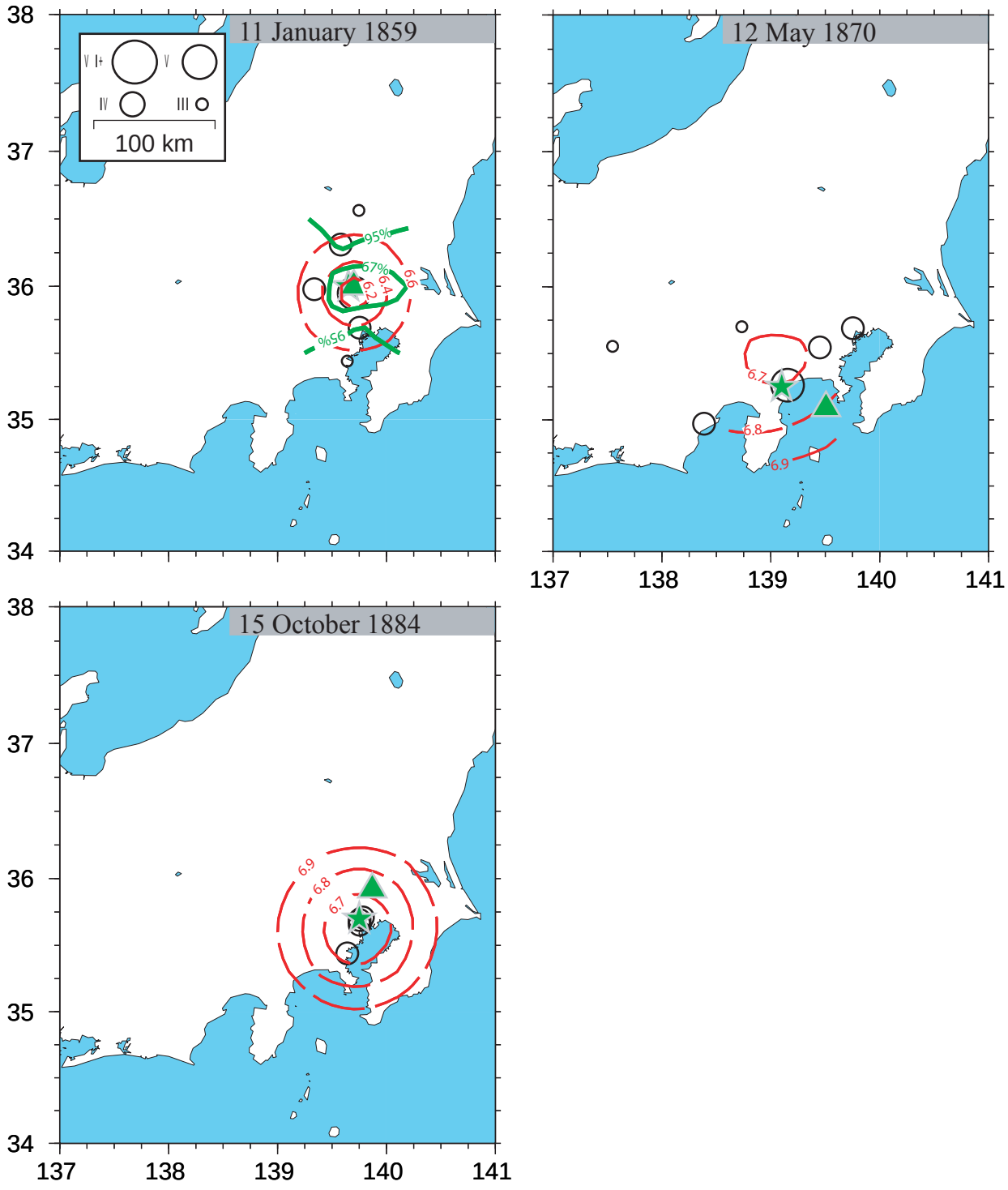
11 January 1859
12 May 1870
15 October 1884
VI+
V
IV
III
100 km
95%
67%
6.2
6.4
6.6
6.7
6.8
6.9
38
37
36
35
34
137
138
139
140
141